DELFT UNIVERSITY OF TECHNOLOGY

FACULTY OF AEROSPACE ENGINEERING

AE4870B

RE-ENTRY SYSTEMS

Assignment IV: Gliding and Skipping Flight

Lecturer: Dr. E. Mooij
Hours spent: 6h
December 16, 2022

Lorenz Veithen 5075211

TU Delft Delft University of Technology

1 Skipping Flight

1.1 First Two Lowest Points

The local minima of the two first skips can be found and compared to their theoretical value in Table 1, characterised based on the altitude and velocity of the vehicle. The theoretical values are obtained based on Equations (1) and (2).

$$h_p = -H_s \ln\left(\frac{4(W/S)}{H_s g \rho_0 C_L}\sin\left(\frac{\gamma_E}{2}\right)^2\right) \quad (1) \qquad V_p = V_E e^{\frac{\gamma_E}{L/D}} \quad (2)$$

The purely theoretical approach consists in assuming a conservation of the entry angle magnitude for each skip, implying that exit flight path angle $\gamma_F = -\gamma_E$ (the magnitude of the exit angle of the atmospheric phase is equal to the entry angle). Using Equation (1), the same altitude is obtained for the lowest point of each skip. The velocity at those points is obtained using Equation (2) for the first skip, and $V_p = V_E e^{\frac{3\gamma_E}{L/D}}$ for the second (the velocity is attenuated during the first entry, the first ascent and the second entry prior to reaching that point). The theoretical approach therefore describes a system in which the velocity is reduced at each skip from the friction with the atmosphere, but the minimum altitude of each skip remains constant until a complete capture of the atmosphere occurs. In practice, as seen below, the altitude of the lowest point slightly varies between the two skips, as a result from the loss of energy occurring during the assumed frictionless part of the flight in the theoretical model ($h > h_E$). The results for both the theoretical and numerical approaches are given in Table 1.

Table 1: Altitude and velocity at the lowest point of the first and second skips.

	Skip 1		**Skip 2**	
Variable	h_p [km]	V_p [km/s]	h_p [km]	V_p [km/s]
Numerical Value	55.1845	7.4699	55.0226	6.3675
Theoretical Value	55.0800	7.3957	55.080	6.321

Considering the first skip, it can be seen from Table 1 that the error in the estimate of the analytical model for h_p and V_p are only about -0.19% and -1% respectively, meaning that the assumptions ($L >> W$ and $D >> W$, and entry at 120 km, atmosphere neglected above) taken in the derivation of those expressions are accurate. Considering the second skip, the theoretical approach results in a deviation from the numerical model of 0.1% and -0.7% for h_p and V_p respectively, which is an even lower error than for the first skip. Another approach which could be considered to further improve the results consists of using the actual entry conditions of the second skip as input to Equations (1) and (2). Defining the entry as the point $h = h_E$ after the exo-atmospheric phase, this results in $h_p = 57.256$ km and $V_p = 6.3713$ km/s. The error in the altitude of the lowest point then grows to 4% for the second skip, but the velocity at that point is estimated with an accuracy of 0.06%: a better estimation of the velocity is reached at the cost of a worse one for the altitude, probably arising from the ambiguous definition of the entry conditions. Nevertheless, it can be concluded that the purely theoretical model is sufficiently accurate for design purposes, in comparison to the numerical model.

1.2 Exit Conditions After Each Skip

The exit conditions can be considered in two manners: either by taking the first point for which the altitude is larger than the entry altitude ($h \geq h_E$), or the point for which the flight path angle reaches a local maximum (as it would theoretically be $-\gamma_E$ at exit, although this is never reached due to energy losses). The data points relative to the two approaches is given in Tables 2 and 3.

Table 2: Exit conditions of skips 1 and 2 for $h \geq h_E$.

# Skip	h_e [km]	V_e [km/s]	γ_e [°]	Δt [s]
1	119.995	6.819	7.694	133.69
2	119.992	5.759	5.255	174.99

Table 3: Exit conditions of skips 1 and 2 for γ a local maximum.

# Skip	h_e [km]	V_e [km/s]	γ_e [°]	Δt [s]
1	79.981	6.878	8.390	92.149
2	73.484	5.855	7.857	106.299

The theoretical values for the entry conditions at the end of the first and second skip are given by $\gamma_F = 9°$, $h_F = 120$km, with $V_{F,1} = 6.837$ km/s and $V_{F,2} = 5.843$ km/s for the first and second skips respectively. Comparing the two approaches (definition based on γ or h), it is clear that the points considered by each are very different (from the altitude difference), but the velocity change from the point of largest γ and the point of $h \approx 120$km is only of the order of 1-2%. The difference in the magnitudes of the flight path angle, however, are quite significant. Furthermore, the analytical model does not estimate either of the approaches significantly better than the other in terms of the velocity magnitude (error is always in the 0.5-1% range). Overall, it may be preferred to use the definition based on the flight path angle, as γ reaching a local maximum has more physical meaning than setting the entry at a relatively arbitrary altitude. Concluding, the analytical model provides a good estimation of the velocity in all cases and can be used for preliminary design purposes.

1.3 Sensitivity to Vehicle Design and Entry Conditions

The effects of the mass m_V, lift-to-drag ratio and entry flight path angle, on the trajectory and thermo-mechanical loads are studied through Figures 1, 2 and 3. The effect of each parameter is considered individually in the following discussion.

An increase in C_L/C_D results in an increase of the maximum altitude reached during the exo-atmospheric flight phase; an increase of the velocity at which the vehicle leaves the atmosphere; and an increased minimum altitude in each skip (Figure 1a). Additionally, the maximum g-load decreases slightly for increasing C_L/C_D from 11.6 to 11.1 on a 50%

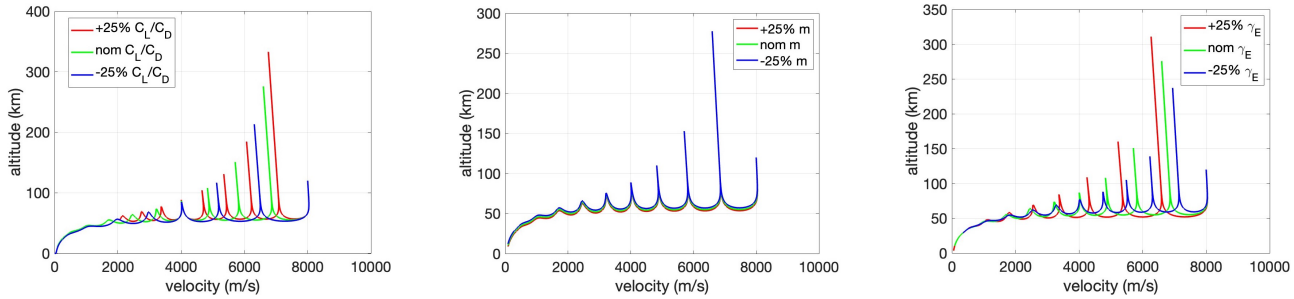

(a) C_L/C_D variation. (b) m_V variation. (c) γ_E variation.

Figure 1: Trajectory changes for variations of $\pm 25\%$ in C_L/C_D, m_V and γ_E.

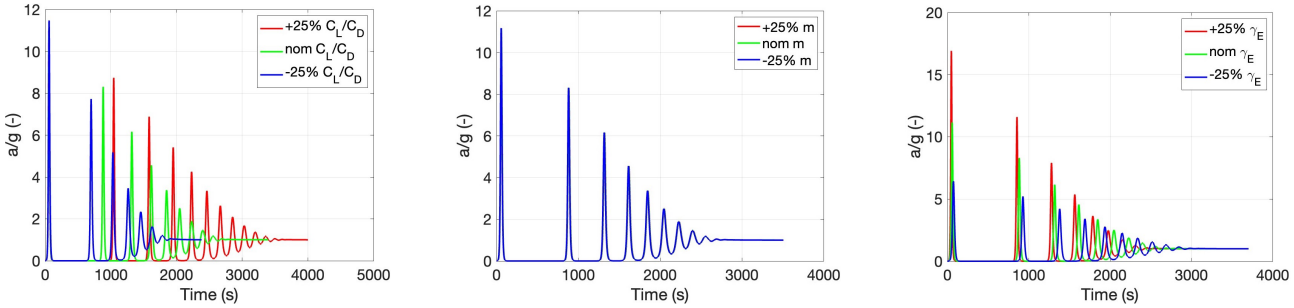

(a) C_L/C_D variation. (b) m_V variation. (c) γ_E variation.

Figure 2: G-load changes for variations of $\pm 25\%$ in C_L/C_D, m_V and γ_E.

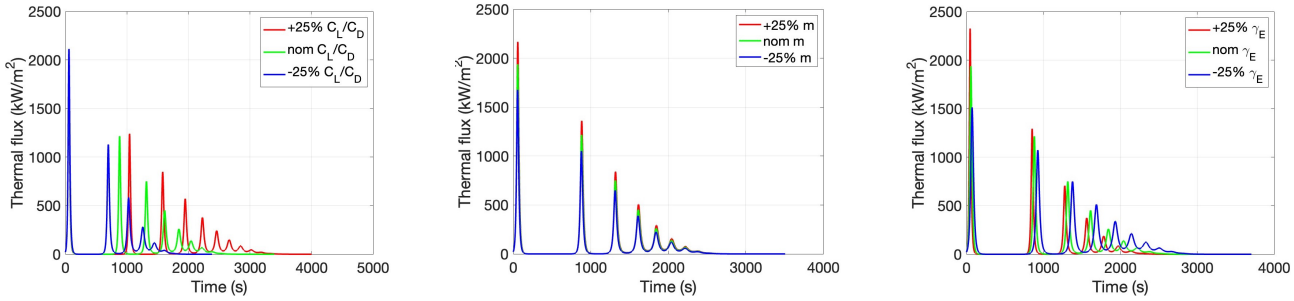

(a) C_L/C_D variation. (b) m_V variation. (c) γ_E variation.

Figure 3: Stagnation thermal flux changes for variations of $\pm 25\%$ in C_L/C_D, m_V and γ_E.

range), occurring essentially at the same time of flight. The following peaks, however, are higher for higher values of C_L/C_D, and occur at the same intervals as the skips (skips are shorter in time for lower values of C_L/C_D; Figure 2a). Furthermore, a similar behaviour as for the g-load is observed for the thermal flux, but q_c becomes insignificant earlier in the flight (Figure 3a). Physically, this behaviour can be explained as follows: a larger C_L/C_D for the same C_D gives an increased lift coefficient; for an increased C_L, the minimum points of the skips occur higher as less density is necessary to generate the same lift (which shifts up the altitude-velocity profile). The lowest point occurring higher, the exit velocity of a given skip is larger as the vehicle was only exposed to lower density layers of the atmosphere (hence losing less energy), which results in a higher altitude during the exo-atmospheric phases. The $q_{c,max}$ and $n_{g,max}$ are originally reduced due to the skip out before reaching the denser layers of the atmosphere in the first skip, but the following peaks are higher because the vehicle re-enters the atmosphere at significantly higher velocities compared to the nominal case.

An increase in the vehicle's mass m_V provides the vehicle with a larger inertia, the lowest points of the skips will be shifted down, as it requires "more atmosphere" to give the same upward movement to the vehicle. Additionally, the vehicle will have gone through more atmosphere and less friction, resulting in a lower exit velocity of the skips and a lower maximum altitude during the phases outside of the atmosphere (Figure 1b). Furthermore, as a vehicle with a larger mass reaches lower altitudes during each skip, the thermal loads endured are also higher (due to the increased density), as seen on Figure 3b. Following, the g-load endured by the vehicle is independent from the mass at all times (as was seen in assignment III), meaning that the only effect of the change in m_V on Figure 2b is that of very slight shifting in time due to difference in trajectory: the larger the mass, the longer the flight and the later in absolute time the peak in g-load.

An increase in the absolute value of γ_E results in an entry that is less shallow, which means that lower altitudes are reached before the lift of the vehicle overcomes its inertia and it gains altitude again (lower altitude of the lowest points in the skips; Figure 1c). This also results in a larger energy loss, meaning that the exit velocity of each skip is smaller. However, the increase in $\gamma_F = -\gamma_E$ is large enough to compensate and overcome this loss in exit velocity, such that a larger maximum altitude is reached during the exo-atmospheric phase. Furthermore, similarly to the earlier cases, both

$n_{g,max}$ and $q_{c,max}$ are larger for an increased entry angle magnitude, as seen from Figures 2c and 3c. However, the trajectory terminates earlier for larger γ_E magnitude, meaning that the red peaks damp faster than the other ones.

When it comes to design purposes, it must be noted that mainly the maximum value of the thermal flux q_c and g-load a/g (and their respective altitude of occurrence), are important for the mission and vehicle design. Therefore, in general an increase C_L/C_D would be preferred to reduce the maximum loading on the system. However, that comes at the cost of a trajectory containing much larger skips. The effect of the mass is generally smaller than the two other parameters, but lowering the mass can help reduce the q_c on the system (although this also comes at the cost of (slightly) more significant skips). Finally, a lower entry angle magnitude γ_E results in a smaller thermo-mechanical loading and less significant skipping. Based on those conclusions, the vehicle can be fitted to achieve a desired entry trajectory design: for example, if a too large skip at the start of the trajectory violates the entry corridor constraints, it might be worth reducing C_L/C_D and γ_E, if allowed by the vehicle's ability to handle the thermal and structural loadings, to reduce the need for heavy controls.

2 Entry Corridor

The entry corridor describes the space of allowable trajectories in the altitude-velocity graphs, that ensure a safe atmospheric entry. For the preliminary design of re-entry trajectories, three constraints are considered. *1.* The equilibrium glide condition, which is the theoretical limit under which no skipping flight will occur (the vehicle will not shoot back up into space). The constraint line is obtained from Equation (3). *2.* The stagnation heat flux experienced during the entry gives the second major limit, above which the vehicle's trajectory shall remain in the h-V plot, from the maximum thermal flux that the vehicle can experience: $q_{c,max}$. The constraint line is given by Equation (4), note that m and n are constants for the Chapman heat flux model. *3.* The last constraint considered arises from the maximum g-load that the vehicle can endure without failure (or that on-board astronauts can survive reasonably), $n_{g,max}$. This translates to a line above which the vehicle's trajectory shall remain, given by Equation (5).

$$h_{eq} = -H_s \ln\left(2\frac{m_V g/S_{ref}}{C_L \rho_0}\left(\frac{1}{V^2} - \frac{1}{V_c^2}\right)\right) \quad (3) \qquad h_{q_c} = -H_S \ln\left(\left[R_N^m \frac{q_{c,max}}{c^*}\left(\frac{V_c}{V}\right)^m\right]^{\frac{1}{1-n}}\right) \quad (4)$$

$$h_g = -H_s \ln\left(\frac{2n_{g,max} m_V g_0}{\rho_0 V^2 S_{ref}\sqrt{C_D^2 + C_L^2}}\right) \quad (5)$$

When it comes to the design of an entry mission and/or vehicle, those constraints directly impact the trajectory design, which poses direct requirements on the the guidance and control systems of the vehicle. It is therefore useful to study the effects of the lift coefficient C_L (considered by applying a variation to the lift-to-drag ratio), mass m_V, nose radius R_N, reference surface area S_{ref} and the maximum g-load $n_{g,max}$ and thermal flux $q_{c,max}$ constraints, on the entry corridor. This is done by varying each parameter by $\pm 25\%$ and considering the effect on each constraint.

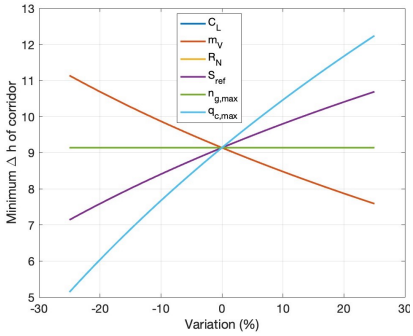

Figure 4: Minimum width of the corridor.

Table 4: Mean percentage variation of the altitude of the constraints of equilibrium glide, maximum thermal heat flux and g-load, over the 2 - 7 km/s velocity range, for a 25% increase in the variables C_L, m_V, R_N, S_{ref}, $n_{g,max}$ and $q_{c,max}$ (one at a time).

	C_L	m_V	R_N	S_{ref}	$n_{g,max}$	$q_{c,max}$
h_{eq}	2.3497	-2.3497	0	2.3497	0	0
h_{q_c}	0	0	-3.4641	0	0	-6.9282
h_g	2.4629	-2.9582	0	2.9582	-2.9582	0

The general behaviour of the each constraint line with respect to the selected parameters, is considered in Table 4 by taking a variation of +25%. For each curve, the mean percentage change in altitude over the velocity range is given (only velocities between 2 and 7 km/s were considered as all curves are defined in this range), indicating if the constraint moves up (positive) or down (negative) in the altitude-velocity graph. Note that in general, an increase in h_{eq} and a decrease in both h_g and h_{q_c} result in a relaxation of the constraints for the trajectory. The following points are noted on those behaviours:

- The upper constraint given by the equilibrium glide condition h_{eq} shows a dependence on the lift coefficient, mass of the vehicle, and the lifting surface area from the considered variables, as can be seen from Equation (3) and Table 4. Note, that both the C_L and S_{ref} variations cause the same curve shift, as can clearly be seen from Equation (3) (both in denominator). Essentially, an increase of either S_{ref} and C_L result in a smaller required density to glide at the same speed (from $L = \frac{1}{2}C_L \rho V^2 S_{ref}$). This results in an upward (relaxation) shift of the curve. Furthermore, an increase in the vehicle's mass results in a shift down of the h_{eq} curve. This is a result from the larger weight that is to be counteracted, meaning that (for the same velocity, C_L and S_{ref}), a larger density is required to glide, which results in a shift down of the equilibrium glide curve.
- Considering the constraint relative to the maximum thermal flux endured by the vehicle, it can be seen that it only depends on the nose radius and the aforementioned constraint (in the considered parameters). Equation (4) and Table 4 show that an increase in either of those results in a shift down of the curve, and therefore a relaxation of the constraint. The physical mechanism is obvious for $q_{c,max}$, which indicates the maximum stagnation thermal fluxes

(a) Altitude-velocity profile.

(b) Flight path angle as a function of time.

Figure 5: Trajectory in terms of the altitude-velocity profile and flight path angle as a function of time for $\sigma = 0°$ and $\sigma = 60°$.

the vehicle can endure: an increase in $q_{c,max}$ results in a larger domain of trajectories are feasible. Furthermore, from hypersonic aerodynamics theory, it is known that the thermal flux endured by a vehicle is reduced for larger R_N. Meaning that, for an increased R_N, the stagnation thermal flux acting on the vehicle for the same trajectory is less and the constraint is weaker.

- The g-load constraint is dependent on C_L, S_{ref}, m_V, and $n_{g,max}$ among the parameters considered, as can directly be seen from Table 4 and Equation (5). The two former result in an upward shift (larger constraint) of the curve essentially from the fact that at the same velocity, with a larger lift coefficient and/or lifting surface, a lower density (altitude) is required to provide the same (maximum) g-load. This is also immediately obvious from $n = \sqrt{C_D^2 + C_L^2}\rho V^2 S_{ref}/(m_V g)$. From the same equation, it is directly seen that an increase in mass will result in a shift down (relaxation of the constraint) of the curve as a larger density is necessary to obtain the same g-load. At last, it is obvious that if the vehicle is able to sustain a larger g-load, the constraint is relaxed, which is translated to a downward shift of the curve.

The minimum width of the corridor, which is the most critical part of the atmospheric entry due to the low margin for error, is investigated by considering Figure 4. Note that the lines relative to R_N and C_L are both directly superposed with the curve of S_{ref}. From this graph, the following can be noted: **(1)** A change in the maximum load factor $n_{g,max}$ has no impact on Δh, simply because the limit arising from the maximum thermal flux which the vehicle can endure is more constraining in the range of velocities (around 6-7 km/s) at which this minimum width occurs. **(2)** An increase in the reference (lifting) surface area S_{ref} results in an increase in Δh and therefore a relaxation of the constraint on the trajectory. This is a direct effect of the moving up of the h_{eq} line discussed above. Furthermore, as already noted above, the lift coefficient has the exact same influence on h_{eq}. Although they also have a contribution on h_g (decoupled this time), h_g has no impact on Δh in this configuration, as seen above. **(3)** A variation of the mass of the entry vehicle causes a reduction of the minimum width of the corridor, making this phase of the trajectory more critical. This is also seen from its direct effect as a shift down of the h_{eq} curve while not affecting the h_{q_c} one. **(4)** Obviously, an increase in the ability of the vehicle to sustain the stagnation thermal flux, $q_{c,max}$, results in a reduced constraint and an increased Δh. This was also already seen from Table 4. **(5)** The effect of R_N on Δh is found to be very similar to the one of S_{ref} and C_L, the curves are indistinguishable in the figure as they are only very slightly different. An increase in the nose radius shifts down the lower boundary of the minimum width region of the corridor, which relaxes the constraints on the trajectory and results in a larger Δh.

To conclude, it was seen that the effect of the parameters on Δh and h_g are opposite: a relaxation of one will be restraining the other. In general, it comes down to finding an optimum based on the five vehicle parameters considered to reach a safe entry corridor. In case the minimum width of the corridor needs to be increased because it is too critical, the C_L, R_N, S_{ref} should be increased and the vehicle's mass should be decreased. However, this results in a more constraining g-load curve towards the end of the flight (except for R_N which only influences Δh here), which needs to be analysed to ensure feasibility. If the later portions of the flight are posing problems, the opposite actions can be taken on the same parameters. Additionally, more robust thermal and structural designs of the vehicle would generally permit higher g-and thermal loads, which would also reduce the constrains (except if astronauts are on-board, where the g-load limit cannot be worked on).

3 Guidance

In this section, the effect of changing the bank angle, σ, from 0°to 60°is considered, although the value is kept constant during each individual run. The bank angle directly results in a decrease in vertical lift force during the flight, which permits to avoid a skipping flight and ensure a gliding one (if done properly). The atmospheric entry trajectories and thermo-mechanical loads issued from having $\sigma = 0°$ and $\sigma = 60°$ are given in Figures 5 and 6. The analysis was performed with $\gamma_E = -2°$, $S_{ref} = 50$ m^2 and $m_V = 2000$ kg.

First considering the overall trajectory, it can be seen from the flight path angle plot that the entry taken with a bank angle of 60°is significantly shorter than the one with $\sigma = 0°$. This is a direct result from the tilt of the lift vector out-of-plane, reducing the vertical component of the resultant aerodynamic force. This reduces the ability of the vehicle to sustain prolonged gliding flights, reducing the flight time, from about 5000s to 2800s, and range, from 27.279 km

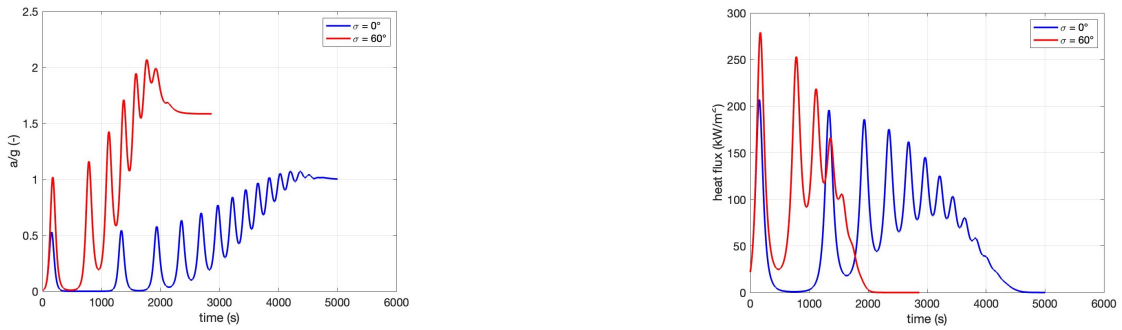

(a) G-load as a function of time.

(b) Thermal flux as a function of time.

Figure 6: Thermo-mechanical loads for $\sigma = 0°$ and $\sigma = 60°$.

to 11.560 km. This is especially important when considering the design of the entry trajectory for a specified landing location: a bank angle profile will permit to stay within the entry corridor, but has a direct impact on the landing location. Following, it can be seen from Figure 5a that the skips resulting from the higher bank angle flight reach smaller altitudes in their ballistic phase, have a lower minimum altitude, and damp out to a gliding flight much faster. Physically, this arises from the reduced vertical component of the lift vector, meaning that the vertical motion is reduced and lower altitudes are reached during the descent phase of the skip before the lift vector is large enough to overcome the vehicle's downward motion. This can be desired for the design of the entry trajectory as it is closer to being within the entry corridor, although some work is still necessary on the control perspective. Furthermore, it can be seen that the flight path angle converges to different values towards the end of the flight, showing that not all the horizontal velocity is lost due to the magnitude lift component (which is different from one configuration to another resulting in different final values).

The thermo-mechanical loads are plotted with respect to time in Figure 6. Comparing the stagnation heat flux acting on the vehicle for $\sigma = 0°$ and $\sigma = 60°$, it is obvious that $q_{c,max}$ is significantly larger for a larger constant bank angle. This results from the reduced vertical lift, which allows the vehicle to reach lower altitudes with velocities only slightly lower than in the case of $\sigma = 0°$, meaning that the dynamic pressure and resulting thermal loading is higher. The oscillations in Figure 6b refer to each skip, with a local maximum reached during the descent of the vehicle each time. Similarly, the g-load experienced through the flight is generally higher for $\sigma = 60°$ than for $\sigma = 0°$, also with oscillations referring to the skips. The same reason generally applies for the increased g-load, as for q_c, however it is clear that for the given vehicle configuration, the g-loads are generally small and do not come close to the structural or human constraints. Furthermore, it must be noted that the converged value (for the final part of the flight), is different from one bank angle to the other.

From this bank angle control experiment, it can be concluded that σ has a significant effect on both the trajectory and the loads. A smaller bank angle will generally result in smaller thermo-mechanical loads but also increases the maximum altitude of the skips and the number of them; while a larger bank angle does the exact contrary. Therefore, alternating between different values of σ would permit to control the overall trajectory to ensure a safe descent by fitting the trajectory within an entry corridor. Especially at the the start of the entry, where the largest skip needs to be controlled to avoid escaping the atmosphere again, by setting a large σ.

4 Mission Design

This section aims to design an entry trajectory which fits within the entry corridor discussed earlier, for the configuration already mentioned in the previous section: $\gamma_E = -2°$, $S_{ref} = 50$ m^2 and $m_V = 2000$ kg. The trajectory shown by Figure 7 and associated bank angle control from Figure 8 were obtained through trial and error using the following principles. Note that the number of controls was aimed to be minimised for simplicity of the system.

1. As already mentioned previously, the bank angle directly controls the vertical component of the lift, and therefore provides control on the vertical motion of the vehicle. The closer to $\sigma = 0°$, the more lift acts on the vehicle and the higher it will reach during the next skip. The closer to $\sigma = 90°$, the less lift (exactly $90°$ is essentially a ballistic flight) and the lower (if at all) the vehicle will go during the next skip. Those principles can generally be used to ensure that the more lift is generated when the vehicle comes close to the lower constraint of the corridor and the oppposite for the upper one.
2. A large bank angle is desired at the start of the entry, where the vehicle has the most kinetic energy and the largest skip would occur. It is therefore required to ensure that the vehicle dives enough in the atmosphere to reduce its energy sufficiently, such that it does not rise past the equilibrium flight constraint. A large bank angle then reduces the vertical lift force, which permits to dive deeper in the atmosphere before the vehicle rises up again. $\sigma = 80-90°$ was found to be sufficient to reduce the first skip below the gliding flight equilibrium constraint, effectively keeping the vehicle in the atmosphere.
3. Following, the bank angle needs to be increased to ensure that the vehicle does not cross the thermo-mechanical constraints imposed by the corridor. In the trajectory shown here, this is done in a gradual fashion, by lowering $\sigma = 85°$ at $t = 100$s within the flight to $\sigma = 60°$ at $t = 500$s. This gradual change in bank angle permits to lower the pressure on the control surfaces and reduce the number of inputs to obtain a feasible trajectory.
4. In a general manner, it is important to realise that the response of the system is not immediate and takes time to build up due to the inertia of the vehicle when the control is applied. This means that, for example, a control aiming

to go make the vehicle gain altitude (lowering σ) needs to applied earlier than the point where the trajectory crosses the bottom constraint of the corridor (being either from $q_{c,max}$ or $n_{g,max}$. Furthermore, the ability of the control surfaces to rotate the spacecraft should be taken into account in further design phases as going from $\sigma = 0°$ to $\sigma = 90°$ within 5 seconds might be unfeasible.

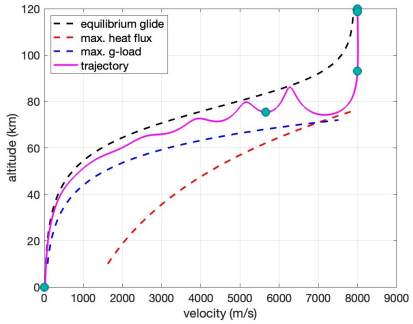

Figure 7: Trajectory controlled through bank angle variations to ensure a safe descent through the entry corridor. Bullets indicate the control points defined.

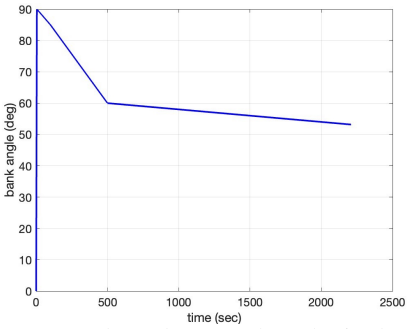

Figure 8: Bank angle control to obtain the safe trajectory, within the constraints of the entry corridor.